

Properties of slow magnetoacoustic oscillations of solar coronal loops by multi-instrumental observations

2 V. M. NAKARIAKOV,^{1,2} M. K. KOSAK,¹ D. Y. KOLOTKOV,¹ S. A. ANFINOGENOV,³ P. KUMAR,⁴ AND Y.-J. MOON²

3 ¹*Centre for Fusion, Space & Astrophysics, Physics Department, University of Warwick, Coventry CV4 7AL, UK*

4 ²*School of Space Research, Kyung Hee University, Yongin 17104, Korea*

5 ³*Institute of Solar-Terrestrial Physics SB RAS, Lermontov St. 126, Irkutsk 664033, Russia*

6 ⁴*Heliophysics Science Division, NASA Goddard Space Flight Center, Greenbelt, MD 20771, USA*

7 ABSTRACT

8 Rapidly decaying oscillations of the thermal emission detected in the decay phase of solar
9 and stellar flares are usually interpreted as standing or sloshing (reflecting) slow magneto-
10 acoustic oscillations. We determine the scalings of the oscillation periods, damping times and
11 amplitudes with the temperature, considering both standing and sloshing oscillations detected
12 with different instruments. In addition, the time evolution of different spatial harmonics of
13 a sloshing oscillation is considered. Parameters of slow oscillations observed in the EUV,
14 X-ray, and microwave bands, and published in the literature, are used. The damping time of
15 slow oscillations is found to scale almost linearly with the oscillation period, as the period
16 to 0.87 ± 0.1 , giving the average Q-factor determined as the ratio of the damping time to the
17 period, of about 1. The Q-factor is found to scale with the relative amplitude to the power
18 of $0.33^{+0.10}_{-0.11}$ with 95 % confidence. The amplitudes of different spatial harmonics forming a
19 sloshing pulse show similar time evolution, suggesting that the period-dependent dissipation
20 is counteracted by another mechanism. The results obtained indicate that the damping of
21 slow oscillations depends on the oscillation amplitude, and that the competition of nonlinear

and dissipative effects could allow for the existence of wave pulses of a sustained shape.

Keywords: Sun: corona — Sun: oscillations

1. INTRODUCTION

Slow magnetoacoustic oscillations of solar coronal loops, also often called “SUMER” oscillations, as they were discovered as periodic variations of the Doppler shift of hot emission lines with the high-resolution imaging spectrometer SOHO/SUMER (e.g., Wang et al. 2002) remain a popular research topic. In particular, the interest in SUMER oscillations is connected with the seismological estimation of the plasma- β and magnetic field in oscillating loops (Wang et al. 2007), and possible diagnostics of the coronal heating function (Nakariakov et al. 2017). Properties of SUMER oscillations may indicate the suppression of thermal conduction along the field (Wang et al. 2015, 2018). There is also a growing interest in the possible association of several-minute quasi-periodic pulsations detected in stellar flares with slow oscillations (see, e.g., Van Doorselaere et al. 2016; McLaughlin et al. 2018, for recent reviews), which would provide us with the solid basis for the exploitation of the solar-stellar analogy (Cho et al. 2016; Kolotkov et al. 2018).

SUMER oscillations of coronal loops are characterised by relatively long periods, from a few minutes to a few tens of minutes, which correspond to the acoustic travel time along the oscillating loop; a very rapid damping, with a ratio of the damping time to the oscillation period of about unity; and a large relative amplitude that is more than 10% of the local sound speed (see Wang 2011, for a comprehensive review). The damping time of SUMER oscillations is found to scale linearly with the oscillation period (Wang et al. 2003; Mariska 2006). The quarter-period phase lag between velocity and intensity disturbances, detected in some cases (e.g., Wang et al. 2002), unequivocally indicate that SUMER oscillations are produced by a standing slow wave, at least in those cases.

Oscillatory phenomena similar to SUMER oscillations, have been observed with several other instruments. Mariska (2005, 2006) detected decaying oscillations in Doppler shifts in the S XV and Ca XIX emission lines observed with Yohkoh/BCS. The quarter-period phase shift between the Doppler-shift and intensity oscillations was detected in some cases, similar to this detected with SUMER. Mariska et al. (2008) studied a 35-min Doppler shift oscillation in the Fe XII–Fe XV emission lines with Hinode/EIS. The oscil-

48 lations in the lower temperature lines rapidly decayed, while the oscillation in Fe XV showed no evidence
49 for decay. Despite the decayless behaviour and the relatively low amplitude, of about 1% of the sound
50 speed, the oscillation was interpreted as a standing slow mode. [Srivastava & Dwivedi \(2010\)](#) observed
51 several-minute periodicities of intensity oscillations of Fe XII with Hinode/EIS, interpreted as the superpo-
52 sition of the fundamental and second harmonics of the slow mode. [Reznikova & Shibasaki \(2011\)](#) observed
53 periodic variations of the microwave emission, with period growing from 2.5 to 5 min, with NoRH. [Kim
54 et al. \(2012\)](#) detected decaying 13-min intensity oscillations simultaneously in EUV and microwave, with
55 SDO/AIA and NoRH, respectively. [Kupriyanova et al. \(2014\)](#) interpreted 2-min pulsations of the thermal
56 microwave emission detected with NoRH, as slow oscillations. The pulsations occur to be co-phased along
57 the entire emitting loop, as expected in the fundamental standing harmonic. [Kupriyanova & Ratcliffe \(2016\)](#)
58 found damped one-minute oscillations of the microwave and X-ray emission during the decay phase of a
59 flare, and interpreted it as a fundamental slow mode. [Li et al. \(2017\)](#) studied 10-min oscillations in the
60 Doppler shift and integrated intensity of the Fe XXI emission line observed with IRIS, the soft X-ray flux
61 measured with GOES, and EUV light curves obtained with SDO/AIA.

62 On the other hand, [Kumar et al. \(2013\)](#) observed a travelling intensity perturbation of a hot, 8–10 MK,
63 coronal loop, in a C7.4 class flare, with SDO/AIA. The intensity variation was seen to bounce approximately
64 four times between the loop’s footpoints, before fading, i.e. exhibiting a “zigzag” pattern in a time-distance
65 plot made along the apparent direction of the magnetic field. The oscillation period and decay time were
66 about 630 s and 440 s, respectively. The apparent phase speed was about 460–510 km s⁻¹ which matched
67 the sound speed in the loop. The authors suggested to call this phenomenon a reflecting longitudinal wave,
68 while [Reale \(2016\)](#) introduced a term “sloshing” oscillations for this phenomenon. A similar, bouncing
69 back and forth between the footpoints, EUV intensity perturbation was detected in another C-class flare by
70 [Kumar et al. \(2015\)](#). The period of the oscillation and decay time were about 409 s and 1121 s, respectively.
71 The characteristic phase speed of the wave is about 560 km s⁻¹, which was roughly consistent with the sound
72 speed at the temperature about 10–16 MK. [Wang et al. \(2015\)](#) observed a clear sloshing pattern in the 131 Å
73 intensity oscillation with SDO/AIA. The oscillation period, decay time, and the apparent phase speed were
74 estimated as about 12 min, 9 min, and 500 km s⁻¹, respectively. [Mandal et al. \(2016\)](#) reported a simultaneous

75 observation of a propagating and reflecting intensity disturbance in a hot coronal loop observed in EUV and
76 X-rays with SDO/AIA and Hinode/XRT, respectively. In addition, three other cases of intensity pulses
77 sloshing between footpoints were analysed. In all considered cases the projected travelling speed was found
78 to be lower than the local sound speed, consistent with the slow wave interpretation. Pant et al. (2017)
79 observed anti-phase oscillations of the 171 Å and 193 Å intensity oscillations at two ends of a non-flaring
80 fan loop system observed with SDO/AIA. The oscillation period was estimated to be 27 min, the damping
81 time of 45 min, and the apparent phase speed of about 75 km s⁻¹. The time-distance map made along the
82 loop showed a sloshing (i.e. “zigzagging”) motion pattern. We need to point out that sloshing oscillations
83 are different from another manifestation of slow waves in the corona, propagating (not reflecting) slow
84 waves that are detected in polar plumes and near footpoints of long loops (see, e.g. de Moortel 2009).

85 Numerical modelling of slow oscillations in a coronal loop reproduced main properties of standing
86 (SUMER) and sloshing oscillations, i.e. the observed oscillation period, $P_{\text{slow}} \approx 2L/C_s$, where L is the
87 loop length and C_s is the sound speed; and associated the rapid damping of the oscillation with the effect
88 of thermal conduction (Ofman & Wang 2002). Nakariakov & Zimovets (2011) demonstrated that a similar
89 periodicity could occur in arcades. The preferential excitation of lower, i.e. the fundamental and second
90 parallel harmonics by an impulsive source, was found in, e.g., Nakariakov et al. (2004); Tsiklauri et al.
91 (2004); Taroyan et al. (2005). Effects of the loop curvature were shown to be not strong (e.g., Selwa et al.
92 2007; Ogrodowczyk et al. 2009). The misbalance of the radiative losses and unspecified background coro-
93 nal heating was found to significantly affect the oscillation quality factor (Nakariakov et al. 2017). Finite
94 amplitude effects were shown to result in steepening of the oscillation, increasing the damping (e.g., Ver-
95 wichte et al. 2008; Ruderman 2013; Kumar et al. 2016). Yuan et al. (2015) performed forward modelling
96 of the manifestation of a slow mode of a hot coronal loop in the SDO/AIA and SOHO/SUMER data. Fang
97 et al. (2015) reproduced numerically the phenomenon of a reflecting longitudinal wave in a hot coronal loop
98 in a form of a plasma blob, and synthesised its manifestation in a spectral line. Reale et al. (2018) modelled
99 sloshing oscillations in an extremely long magnetic tube connecting an Orion pre-main sequence star with
100 the surrounding disk. Recently, Wang et al. (2018) performed 1D numerical simulations of sloshing oscilla-
101 tions in a hot coronal loop, and concluded that quick formation of the fundamental standing mode following

102 initially sloshing oscillations could be caused by enhanced compressive viscosity. However, a detailed study
103 of the preferential excitation of either standing or sloshing oscillations has not been performed. Also, the
104 reason why slow oscillations of both kinds are usually detected in the hot plasma emission remains unclear.

105 Both standing and sloshing oscillations are considered to be associated with the slow magnetoacoustic
106 mode. Both these kinds of slow oscillations occur in closed magnetic configurations. Thus, one differ-
107 ence between SUMER and sloshing oscillations is the phase shift between the parallel velocity and density
108 oscillations. In standing slow oscillations, the velocity and density perturbations are phase shifted by a
109 quarter-period, while in the sloshing oscillations these perturbations are either in phase or in anti-phase.
110 This difference is not connected with the structure of the perturbation along the loop, i.e. with the number
111 of parallel harmonics, which composes the perturbation. It is likely that at least some cases of SUMER
112 oscillations could actually belong to the sloshing oscillation class. It is clear that the oscillations could be
113 produced by any perturbation of the plasma pressure or a field-aligned flow, localised either in the loop or
114 at its footpoints, provided the characteristic time of the perturbation is shorter than the acoustic travel time
115 along the loop. Thus, the driver could be a rapid chromospheric or coronal heating event, a jet, or thermal
116 over-stability. But, in many events such impulsive energy depositions were not observed.

117 In this letter we perform statistical analysis of slow oscillations of both SUMER and sloshing type, in-
118 vestigating the relationship between the oscillation periods, damping time, apparent amplitude, and sound
119 speed; and compare the results with properties of sloshing oscillations.

120 2. SCALINGS OF SLOW OSCILLATION PARAMETERS

121 We perform a statistical analysis of the slow oscillation events reported in the literature ([Wang et al. 2003](#);
122 [Mariska 2006](#); [Mariska et al. 2008](#)), selecting only the events with a reported velocity amplitude, altogether
123 93 events. In addition, we included the event described by [Kim et al. \(2012\)](#), in which determining the
124 relative amplitude of the density perturbation is possible. Using it, we estimated the relative velocity pertur-
125 bation by taking that in an acoustic wave the relative density perturbation is equal to the ratio of the velocity
126 perturbation to the sound speed. We also consider sloshing oscillations with the reported parameters taken
127 from [Kumar et al. \(2013, 2015\)](#); [Wang et al. \(2015\)](#); [Mandal et al. \(2016\)](#); [Pant et al. \(2017\)](#). This statistics
128 includes observations of slow oscillations at approximately eight different temperatures, i.e. 14 MK and

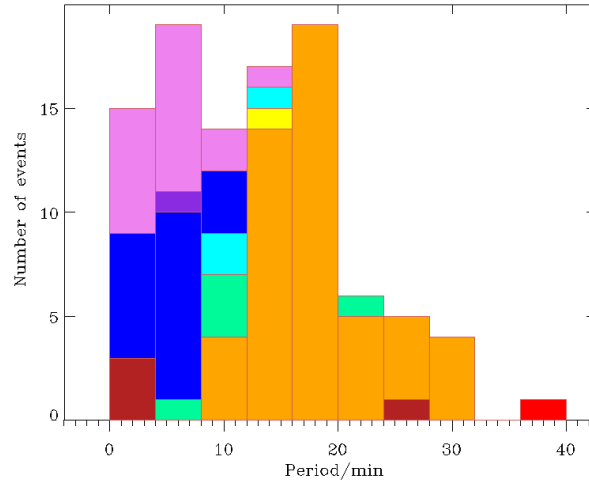


Figure 1. Distribution of the slow oscillation periods for different detection temperatures. The violet colour corresponds to the temperature of 14 MK, magenta to 13 MK, blue to 12 MK, cyan to 10 MK, green to 8.9 MK, yellow to 7 MK, orange to 6.3 MK, red to 2 MK, and brick to 0.6 MK.

129 12 MK with BCS, 13 MK, 10 MK, 7 MK and 0.6 MK with AIA, 8.9 MK and 6.3 MK with SUMER, and
 130 2 MK with EIS, using the estimations found in the papers mentioned above. In all cases, we neglected
 131 finite- β effects, estimating the slow wave speed as $152 \times (T[\text{MK}])^{1/2} \text{ km s}^{-1}$.

132 Figure 1 shows the distribution of the detected periods of both SUMER and sloshing oscillations, with
 133 different colours corresponding to the temperatures associated with the emission lines or bandpasses used
 134 in the detections. The applied colour scheme corresponds to a rainbow, i.e. the violet colour represents
 135 the highest temperature, and the brick colour the lowest temperature. It is evident that the detections in the
 136 hotter channels correspond to systematically shorter oscillation periods.

137 Figure 2 shows the scaling of the damping time with the oscillation period and the plasma temperature. It
 138 is clear that the decay time is apparently proportional linearly to the oscillation period. The scaling of the
 139 decay time τ_D with the period P was obtained by fitting a functional form $\tau_D = CP^p$, where C and p are
 140 constant, into the observational data, using Bayesian inference and Markov chain Monte Carlo (MCMC)
 141 sampling (see Pascoe et al. 2017, for the description of the method). The best fitting values are found to
 142 be $C = 1.18 \pm 0.4$ and $p = 0.87 \pm 0.1$, where uncertainties are estimated at the half levels of the Gaussian
 143 functions best-fitting the corresponding marginal posterior distributions. We need to point out that the

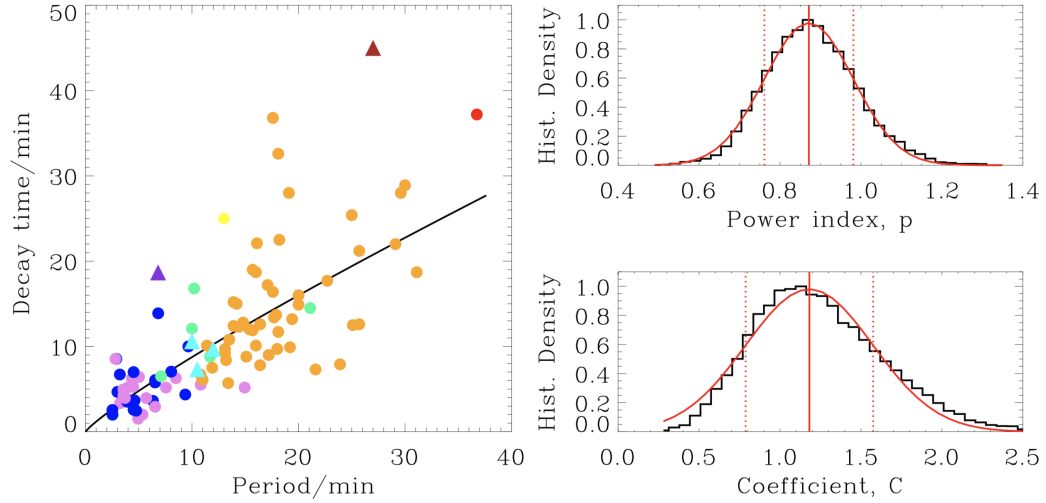


Figure 2. Left panel: Scaling of the damping time of slow oscillations with the period. The colours represent different temperatures as described in Fig. 1. The circles show SUMER oscillations; and triangles show sloshing oscillations. The black line indicates the power-law best-fitting. Right panels: marginal posterior distributions for the model parameters p and C , obtained using Bayesian inference and MCMC sampling method. Red solid lines show the approximation of the corresponding distributions by the Gaussian function with the mean value (the vertical solid lines) and the half-level uncertainties (the vertical dotted lines).

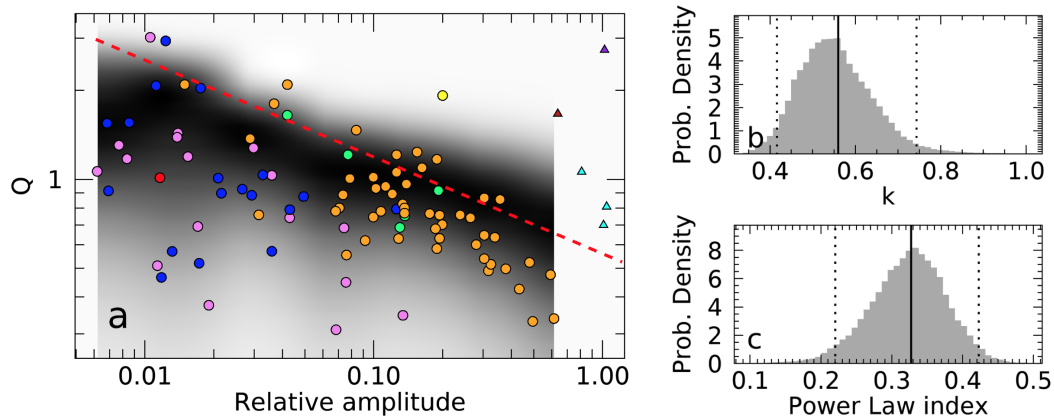


Figure 3. Scaling of the Q-factor versus apparent relative amplitude (a). The data point legend is the same as in Figs. 1 and 2. The red dashed line shows the power law dependence of the Q-factor upon the de-projected amplitude inferred using Bayesian analysis. The background colour shows the posterior predictive probability distribution which highlights areas where data points could be observed according to our model. Panels b and c show marginal posterior distributions for the normalisation constant k and power law index α .

144 marginal posterior distribution of the parameter C shows some deviations from the Gaussian shape, but it
 145 should not strongly affect the estimations. Thus, the results obtained with the extended dataset, including
 146 results obtained with XRT, NoRH and AIA are roughly consistent with the results obtained previously with
 147 SUMER (Verwichte *et al.* 2008) and with SUMER and BCS (Wang 2011), and also in soft X-rays in solar
 148 and stellar flares observed with RHESSI and XMM–Newton (Cho *et al.* 2016). Our value of the exponent,
 149 0.87 ± 0.1 , is close to unity. The large scattering of the data points does not allow one to determine whether
 150 this scaling depends on the specific value of the temperature.

151 We determined the oscillation Q-factor as the ratio of the damping time to the oscillation period, $Q =$
 152 τ_D/P , i.e. the number of oscillation cycles detected in the event. From the fitting shown in Fig. 2, the
 153 Q-factor is seen to weakly depend upon the oscillation period, so that taking the power law index $p \approx 1$, the
 154 value of C could be considered as an average Q-factor of the detected slow oscillations. Sloshing oscillations
 155 are not significantly off the data cloud in this figure, and hence their damping mechanism could be similar
 156 to this of SUMER oscillations.

157 In Figure 3a we plot the Q-factor dependence on the apparent amplitude A , measured in the sound speeds
 158 corresponding to the temperature. In the case of the estimations by the Doppler shift, the amplitude is
 159 affected by the projection effect, and hence one should consider the top-right boundary of the data cloud in
 160 the figure as the actual scaling of the Q-factor with amplitude. A similar technique has been used for the
 161 demonstration of the nonlinear nature of kink oscillation damping by Goddard & Nakariakov (2016). The
 162 data cloud of slow oscillations in the figure clearly has a triangular shape, which indicates the dependence
 163 of the Q-factor on the amplitude, i.e. the nonlinear nature of the damping. We approximated the top-right
 164 boundary of the data cloud in a logarithmic scale by a linear function. In some cases, the relative amplitude
 165 could have an additional error caused by the neglect of finite- β effect, i.e. the amplitude should be measured
 166 not in the units of the sound speed, but of the tube speed. However, this error is not likely to change the
 167 determined scaling qualitatively.

168 For accurate fitting the Q-factor dependence upon the apparent amplitude, we use the following model,

$$Q_i = (k \cos \theta_i) A_i^{-\alpha} + N_i(0, \sigma), \quad (1)$$

169 where Q_i and A_i are the measured Q-factor and relative amplitude for the data point i , and α is the power law
 170 index. The free parameter $N_i(0, \sigma)$ is a normally distributed random “noise” with a standard deviation σ ,
 171 which represents scattering due to the measurement errors and possible dependence upon other properties
 172 of the loops. The projection effect is accounted for by the viewing angle θ_i as a free parameter. Bayesian
 173 inference based on this model revealed that $k = 0.56_{-0.14}^{+0.18}$ and $\alpha = 0.33_{-0.11}^{+0.10} \approx 1/3$ with 95 % confidence. The
 174 marginal posterior distributions for k and α are shown in Fig. 3b and c. The shaded area in Fig. 3a shows
 175 the predictive posterior distribution that demonstrates where the data points could be observed according
 176 our model. Since the true de-projected amplitude (red dashed curve in Fig. 3) corresponds to $\cos \theta = 1$,
 177 observed apparent amplitudes are expected to lie mostly below the curve as we see in our data set.

178 In Fig. 3, we also show sloshing oscillations. Instead of the relative amplitude, for sloshing oscillations we
 179 used their projected phase speed determined by imaging observations. It is done in order to check whether
 180 the evolution of the sloshing blob is indeed produced by the slow wave phase or group speed, or should be
 181 attributed to a bulk flow, as the flows in the SUMER oscillations. The sloshing oscillations (shown by the
 182 triangles) are clearly *off* the data cloud in the figure, indicating that their apparent amplitude corresponds
 183 to the sound (tube) speed, and not the plasma flow speed. Also, it suggests that those slow oscillations that
 184 are *in* the data cloud (the circles), even if their nature was not identified observationally, e.g., because of the
 185 lack of the spatial information, are likely to be of the SUMER type, as it has been previously assumed (e.g.
 186 Wang 2011).

187 3. EVOLUTION OF DIFFERENT SPATIAL HARMONICS

188 Figure 4 shows the evolution of the Fourier amplitudes of the four lowest spatial harmonics in the sloshing
 189 pulse of the EUV emission intensity in the event occurred on 2012 May 7 (Kumar et al. 2013), determined by
 190 the cosine Fourier transform after the subtraction of the mean value from the intensity profile along the loop.
 191 The choice of the basis functions is dictated by the spatial structure of the density (intensity) perturbations
 192 in a standing slow wave. From the analysis, it is evident that the amplitudes of different harmonics of the
 193 sloshing disturbance evolve rather similarly, which indicates that they decay approximately at the same rate,
 194 independent of their wavelengths. Such a behaviour is in apparent contradiction with the results shown in

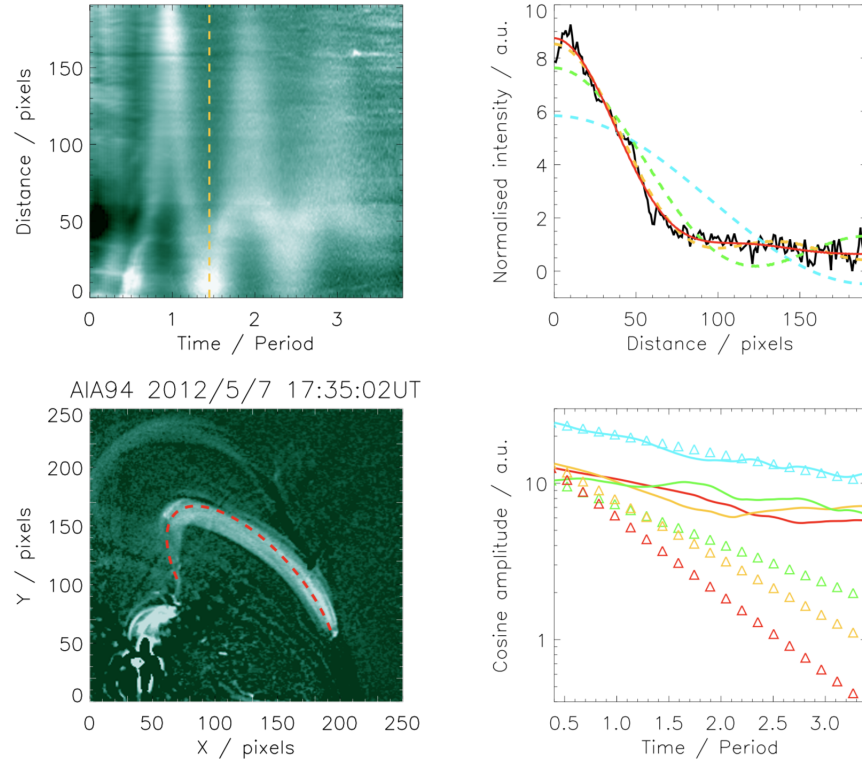


Figure 4. Top left: Time-distance plot made for the slit along the loop shown in the bottom left panel. Each instant of time, the emission intensity is normalised to the mean value over the spatial coordinate. For each pixel, the mean value of the signal over time is subtracted. The time is measured in the units of the detected oscillation period, 630 s. The dashed vertical line indicates a certain instant of time when the signal shown in the top right panel was taken. Bottom left: A snapshot on a sloshing oscillating loop observed by SDO/AIA at 94 \AA . The red dashed line shows the elliptical slit along which the time-distance plot was made. Top right: A snapshot of the variation of the emission intensity along the loop (the black line). The light blue, green, yellow, and red lines show the lowest (fundamental) spatial harmonic, and summations of two lowest, three lowest, and four lowest harmonics, respectively. Bottom right: Variation of the amplitude of the four lowest harmonics with time (solid lines). The blue, green, yellow and red colours indicate the individual four lowest harmonics, respectively. The curves are smoothed with a running average over three oscillation periods. The triangles show the exponential dependence of the amplitudes of the corresponding individual harmonics upon time with the decay time being proportional to the harmonic number, i.e. to the oscillation period.

195 Fig. 2, suggesting the need for the accounting for both the competing effects of wavelength (or period) and
 196 nonlinearity on the damping.

4. DISCUSSION AND CONCLUSIONS

We performed statistical analysis of slow magnetoacoustic oscillations of coronal loops, based on the detections described in the literature, made in the EUV, SXR and microwave bands, corresponding to the plasma temperatures from 0.6 MK to 14 MK. Thus, this study extends the statistical results determined previously for four temperatures by adding five new temperatures. Both standing and sloshing oscillations were considered. It was established that the oscillation period increases with the decrease in the temperature. Previously, this tendency determined by the SUMER and BCS data only, was attributed to the selection effect, as the oscillating loops observed at lower temperatures by SUMER are usually longer (Wang 2011). However, the detections made with AIA, NoRH and XRT seem to correspond to the same pattern: oscillations seen in a hotter plasma have shorter periods, with a few exceptions. Moreover, the newly discovered sloshing oscillations are consistent with this picture too. This behaviour could be attributed to the decrease in the acoustic travel time with the increase in the temperature, i.e. in the sound speed.

All considered oscillation events, including sloshing, are consistent with the linear scaling of the damping time with the oscillation period, established for SUMER and BCS (Wang 2011). More rigorously, the use of the MCMC technique gives that the damping time scales with the oscillation period to the 0.87 ± 0.1 at the half-level of a Gaussian fit, with the Q-factor being approximately constant of about unity. The insufficient number of observed events did not allow us to test this scaling for the sloshing oscillations only.

It was recently proposed that the linear scaling of the damping time and period could be attributed to the combined effect of anomalously large compressive viscosity and the Rosner–Tucker–Vaiana scaling (Wang et al. 2018). This suggests that oscillations of shorter wavelengths should decay faster. However, spatially-resolved sloshing oscillations do not show a dispersion of the oscillating pulse. In other words, in the sloshing oscillations, the oscillating pulse remains localised along the loop, and there is no evidence of the preferential damping of the higher spatial spectral harmonics. Similar behaviour is shown by full-scale numerical modelling (Reale 2016) and needs to be understood. This effect was tested by considering the time evolution of different spatial harmonics of a sloshing oscillation observed with AIA. It was found out that four lowest harmonics show similar decay patterns. It may indicate that the enhanced damping of shorter harmonics is counteracted by another mechanism, e.g. nonlinearity. In particular, it could be

224 explained by the competition of the dissipative processes which tend to preferentially damp the shorter
 225 spatial harmonics, and the nonlinearity that leads to the preferential damping of the harmonics with higher
 226 amplitudes and the nonlinear cascade to the higher harmonics.

227 The oscillation Q-factor is found to decrease with the relative amplitude (normalised to the sound speed),
 228 indicating the nonlinear nature of the damping. For the oscillations detected with SUMER, (Verwichte *et al.*
 229 2008) established that the inverse Q-factor depends linearly on the amplitude (see, also Ruderman 2013,
 230 who proposed the quadratic dependence). But, the line-of-sight projection effect was not taken into account
 231 in that study. Our finding, based on the Bayesian statistics shows that the Q-factor is proportional to the
 232 normalised relative amplitude to the power of $0.33^{+0.10}_{-0.11}$ with 95 % confidence. The physical mechanism
 233 responsible for this effect needs to be identified.

234 This work was supported by STFC consolidated grant ST/P000320/1 (V.M.N., D.Y.K.), the BK21 plus
 235 program through the National Research Foundation funded by the Ministry of Education of Korea (V.M.N.,
 236 Y.J.M.), the British Council Institutional Links Programme (M.K.K.), and the Russian Science Foundation
 237 under project No 18-72-00144 (S.A.A.)

REFERENCES

- 238 Cho, I.-H., Cho, K.-S., Nakariakov, V. M., Kim, S., & 249 Kumar, P., Innes, D. E., & Inhester, B. 2013, *ApJL*,
 239 Kumar, P. 2016, *ApJ*, 830, 110 250 779, L7
- 240 de Moortel, I. 2009, *SSRv*, 149, 65 251
- 241 Fang, X., Yuan, D., Van Doorselaere, T., Keppens, R., 252
 242 & Xia, C. 2015, *ApJ*, 813, 33 253
- 243 Goddard, C. R. & Nakariakov, V. M. 2016, *A&A*, 590, 254
 244 L5 255
- 245 Kim, S., Nakariakov, V. M., & Shibasaki, K. 2012, 256
 246 *ApJL*, 756, L36 257
- 247 Kolotkov, D. Y., Pugh, C. E., Broomhall, A.-M., & 258
 248 Nakariakov, V. M. 2018, *ApJL*, 858, L3 259
- Kumar, P., Nakariakov, V. M., & Cho, K.-S. 2015,
ApJ, 804, 4
- Kumar, S., Nakariakov, V. M., & Moon, Y.-J. 2016,
ApJ, 824, 8
- Kupriyanova, E. G., Melnikov, V. F., Puzynya, V. M.,
 Shibasaki, K., & Ji, H. S. 2014, *Astronomy Reports*,
 58, 573
- Kupriyanova, E. G. & Ratcliffe, H. 2016, *Advances in*
Space Research, 57, 1456

- 260 Li, D., Ning, Z. J., Huang, Y., et al. 2017, ApJ, 849, 286
 261 113 287
- 262 Mandal, S., Yuan, D., Fang, X., et al. 2016, ApJ, 828, 288
 263 72 289
- 264 Mariska, J. T. 2005, ApJL, 620, L67 290
- 265 Mariska, J. T. 2006, ApJ, 639, 484 291
- 266 Mariska, J. T., Warren, H. P., Williams, D. R., & 292
 267 Watanabe, T. 2008, ApJL, 681, L41 293
- 268 McLaughlin, J. A., Nakariakov, V. M., Dominique, M.,²⁹⁴
 269 Jelínek, P., & Takasao, S. 2018, SSRv, 214, 45 295
- 270 Nakariakov, V. M., Afanasyev, A. N., Kumar, S., & 296
 271 Moon, Y.-J. 2017, ApJ, 849, 62 297
- 272 Nakariakov, V. M., Tsiklauri, D., Kelly, A., Arber, 298
 273 T. D., & Aschwanden, M. J. 2004, A&A, 414, L25 299
- 274 Nakariakov, V. M. & Zimovets, I. V. 2011, ApJL, 730,³⁰⁰
 275 L27 301
- 276 Ofman, L. & Wang, T. 2002, ApJL, 580, L85 302
- 277 Ogrodowczyk, R., Murawski, K., & Solanki, S. K. 303
 278 2009, A&A, 495, 313 304
- 279 Pant, V., Tiwari, A., Yuan, D., & Banerjee, D. 2017, 305
 280 ApJL, 847, L5 306
- 281 Pascoe, D. J., Anfinogentov, S., Nisticò, G., Goddard, 307
 282 C. R., & Nakariakov, V. M. 2017, A&A, 600, A78 308
- 283 Reale, F. 2016, ApJL, 826, L20 309
- 284 Reale, F., Lopez-Santiago, J., Flaccomio, E., Petralia, 310
 285 A., & Sciortino, S. 2018, ApJ, 856, 51 311
- Reznikova, V. E. & Shibasaki, K. 2011, A&A, 525,
 A112
- Ruderman, M. S. 2013, A&A, 553, A23
- Selwa, M., Ofman, L., & Murawski, K. 2007, ApJL,
 668, L83
- Srivastava, A. K. & Dwivedi, B. N. 2010, NewA, 15, 8
- Taroyan, Y., Erdélyi, R., Doyle, J. G., & Bradshaw,
 S. J. 2005, A&A, 438, 713
- Tsiklauri, D., Nakariakov, V. M., Arber, T. D., &
 Aschwanden, M. J. 2004, A&A, 422, 351
- Van Doorselaere, T., Kupriyanova, E. G., & Yuan, D.
 2016, SoPh, 291, 3143
- Verwichte, E., Haynes, M., Arber, T. D., & Brady,
 C. S. 2008, ApJ, 685, 1286
- Wang, T. 2011, SSRv, 158, 397
- Wang, T., Innes, D. E., & Qiu, J. 2007, ApJ, 656, 598
- Wang, T., Ofman, L., Sun, X., Provornikova, E., &
 Davila, J. M. 2015, ApJL, 811, L13
- Wang, T., Ofman, L., Sun, X., Solanki, S. K., &
 Davila, J. M. 2018, ApJ, 860, 107
- Wang, T., Solanki, S. K., Curdt, W., Innes, D. E., &
 Dammasch, I. E. 2002, ApJL, 574, L101
- Wang, T. J., Solanki, S. K., Curdt, W., et al. 2003,
 A&A, 406, 1105
- Yuan, D., Van Doorselaere, T., Banerjee, D., &
 Antolin, P. 2015, ApJ, 807, 98